Isotope effect for associative detachment: $H(D)^- + H(D) \rightarrow H_2(D_2) + e^-$

K. A. Miller,[1] H. Bruhns,[1,*] M. Čížek,[2] J. Eliášek,[2] R. Cabrera-Trujillo,[3] H. Kreckel,[1,†]
A. P. O'Connor,[1] X. Urbain,[4] and D. W. Savin[1]

[1]*Columbia Astrophysics Laboratory, Columbia University, 550 West 120th Street, New York, New York 10027, USA*
[2]*Charles University Prague, Faculty of Mathematics and Physics, Institute of Theoretical Physics, 180 00 Praha 8, Czech Republic*
[3]*Instituto de Ciencias Físicas, Universidad Nacional Autónoma de México, Ap. Postal 48-3, Cuernavaca, Morelos, 62251, Mexico*
[4]*Institute of Condensed Matter and Nanosciences, Université Catholique de Louvain, Louvain-la-Neuve B-1348, Belgium*

(Received 1 March 2012; published 27 September 2012)

We report experimental and theoretical results for associative detachment (AD) of $D^- + D \rightarrow D_2 + e^-$. We compare these data to our previously published results for $H^- + H \rightarrow H_2 + e^-$. The measurements show no significant isotope effect in the total cross section. This is to be contrasted with previously published experimental and theoretical work which has found a significant isotope effect in diatomic systems for partial AD cross sections, i.e., as a function of the rotational and vibrational levels of the final molecule formed. Our work implies that though the rovibrational distribution of flux is different for AD of H^- + H and D^- + D, the total flux for these two systems is essentially the same when summed over all possible final channels.

DOI: 10.1103/PhysRevA.86.032714 PACS number(s): 34.50.Lf, 52.20.Hv, 95.30.Ft, 97.10.Bt

I. INTRODUCTION

One of the most fundamental systems for atomic collision studies is the associative detachment (AD) reaction

$$H^- + H \rightarrow H_2 + e^- \tag{1}$$

and its isotopic counterpart

$$D^- + D \rightarrow D_2 + e^-. \tag{2}$$

Only recently, after more than 40 years of effort, have experiment and theory finally converged for reaction (1) [1–3]. However, we know of no published experimental data for reaction (2) and of theory only the results for the 14–17 meV center-of-mass energy range, displaying a small resonance behavior [4].

There are good reasons to suspect an isotope effect in the partial AD cross sections for reactions (1) and (2). For the same collision energy, D moves more slowly than H and penetrates less deeply into the electron cloud of the anion before detachment occurs. The resulting deuterated molecule forms at higher internuclear distances and higher vibrational levels than for the undeuterated molecule [5]. This was seen by the only experimental AD studies we know of which investigate the isotope effect for two-atom collision systems [5,6]. In Ref. [5] experimental and theoretical work was carried out for AD of H and D with Cl^- and Br^- by measuring the relative cross section as a function of the detached electron energy. For AD of $H + F^-$ and $D + F^-$ [6] the relative vibrational level v populations of the resulting HF and DF were determined by measuring the infrared spectra from the excited rovibrational states. These results were supported by later theoretical work [7]. All of these works found a pronounced isotope effect in the partial AD cross section: higher v levels are populated in the deuterated reactions.

Knowledge of reactions (1) and (2) comes also from studies of the time reversed processes of dissociative electron attachment (DEA), namely

$$e^- + H_2 \rightarrow H^- + H \tag{3}$$

and

$$e^- + D_2 \rightarrow D^- + D. \tag{4}$$

Such results can shed light on the AD process by using detailed balance to map the initial molecular rovibrational state in DEA onto the corresponding final state in AD.

Only a few experimental studies exist for reactions (3) and (4). DEA measurements of D_2 found that the cross section at room temperature is at least a couple orders of magnitude smaller than that for H_2 [8–10]. The molecules in these studies were essentially in their ground rovibrational level, suggesting a strong isotope effect for AD into that level. However, AD proceeds primarily through high rovibrational levels [4]. The v dependence of the DEA cross section was studied experimentally by Ref. [11] who found that DEA for D_2 grew more rapidly with v than that for H_2. Various theoretical studies support this trend (reviewed by Ref. [12]), though [13] found that the isotope effect disappears for $v \gtrsim 9$.

Based on these DEA results, we would therefore expect a strong isotope effect in the partial AD cross sections leading to low-lying vibrational states and a weak effect for higher vibrational states. However, it is not clear *a priori* which trend wins out in the total AD cross section. For example, our AD calculations for a series of hydrogen halides show that the isotope effect becomes more important for heavier halogen anions [14].

The total AD cross section can be analyzed theoretically using classical trajectory theories as well as both a classical and quantum opacity function for a given trajectory or partial wave. These approaches all indicate that the total AD cross sections for reactions (1) and (2) are insensitive to the detailed quantum dynamics in the autodetachment region, which occurs for internuclear distances $R < 3a_0$, and that no isotope effect is expected. Systems entering this region rapidly undergo

*Present address: Inficon GmbH, D-50968 Cologne, Germany.
†Present address: Max-Planck-Institut för Kernphysik, Saupfercheckweg 1, 69117 Heidelberg, Germany.

autodetachment resulting in AD. As a consequence, the total AD cross section can be predicted by just calculating which classical trajectories end up in the autodetachment region.

The radial motion of each trajectory with an impact parameter b and relative collision energy E_r is governed by the effective potential

$$V(b,R) = V_i(R) + \frac{b^2 E_r}{R^2}, \tag{5}$$

where $V_i(R)$ is the interaction potential for $H^- + H$ in the absence of any angular momentum and $b^2 E_r/R^2$ is the centrifugal barrier term. Taking $b_c(E_r)$ as the critical value of the impact parameter at which the centrifugal term just prevents the particles from reaching the autodetachment region, then the total AD cross section can be simply given by the geometric cross section

$$\sigma_{AD} = \pi b_c^2. \tag{6}$$

This model only depends on the particle trajectories. Since these trajectories are a function of energy and not velocity, the resulting cross section is independent of mass. We also note that for some potentials it is easy to derive an analytical expression for $b_c(E_r)$. For example, using the polarization potential $V_i(R) = -\alpha/R^4$ in Eq. (6), where α is the polarizability, yields the Langevin cross section $\sigma_L = \pi\sqrt{4\alpha/E_r}$ [15].

The above classical trajectory analysis assumes that every collision crossing into the autodetachment region contributes to AD. For a slightly more involved treatment we can introduce the opacity function $O(b,E_r)$, which gives the probability of the autodetachment for a collision along a trajectory characterized by a given collision energy E_r and impact parameter b. The AD cross section then reads

$$\sigma_{AD}(E_r) = \int 2\pi b\, O(b,E_r) db. \tag{7}$$

This reduces to Eq. (6) if we assume that $O = 1$ for $b < b_c$ and $O = 0$ otherwise. This is a reasonable assumption for a process characterized by a fast autodetachment rate, but in general the opacity function depends on the particle velocity along the trajectory and may thus exhibit an isotope effect.

The explanation of the near disappearance of the isotopic effect can also be derived from a partial wave expansion in the full quantum mechanical treatment. The formula for the cross section can then be written as

$$\sigma_{AD} = \frac{\pi}{2\mu E_r} \sum_L w_L (2L+1) O_L(E_r), \tag{8}$$

where L is the angular momentum, w_L is a statistical weight factor taking into account both nuclear spin and electronic symmetry, and $O_L(E_r) < 1$ is the opacity for the given partial wave. The opacity function is equal to the detachment probability for each partial wave and can be calculated from the partial S-matrix for AD [7,15].

Although Eq. (8) is the exact formula, it gives very similar results for the total AD cross section as does the classical approach. To see this, again we assume that the opacity is approximately equal to one when the incident partial wave L can overcome the centrifugal barrier

$$\frac{L(L+1)}{2\mu R^2} = \frac{b^2 E_r}{R^2}, \tag{9}$$

and enter into the autodetachment region. The opacity is also assumed to be zero when the incident partial waves are shielded from this region. Ignoring the L dependence of the factor w_L, the sum over L produces the factor L_c^2, where L_c is the critical value of L for which O_L vanishes. Using the classical relation between the angular momentum and the impact parameter

$$L_c = b_c\sqrt{2\mu E_r}, \tag{10}$$

one can readily transform Eq. (8) to Eq. (6). The inclusion of the L dependence of w_L, the discrete nature of L_c, and the exact form of O_L all produce a small isotope effect as we will discuss in detail in a subsequent paper focusing on the theory of the reaction.

We conclude that when the opacity function is one for small L and switches rapidly to zero at a certain critical value of L, then both classical and quantum reasoning predicts there will be no isotope effect in the total AD cross section. Such behavior of the opacity function is not automatic as can be demonstrated for the case of hydrogen halides [7]. The opacity function can be expected to switch rapidly from one to zero only if the region of internuclear distances where autodetachment is fast is followed almost immediately by a region where autodetachment is forbidden. Regions of internuclear distances with weak autodetachment would lead to mass dependence in the opacity function and thus to an isotope effect in the total AD cross section.

In an attempt to test these simple theoretical predictions for the isotope effect in the total AD cross section, we have performed both laboratory measurements and fully quantum mechanical theoretical calculations of the total cross section for reaction (2) versus relative collision energy E_r. Our experimental and theoretical approaches have been previously described in detail in Refs. [1–4,16]. Here we give only brief overviews of each.

The rest of this paper is organized as follows. In Sec. II we describe the experimental method. Section III presents our theoretical calculations. We present and discuss our results in Sec. IV. A summary is given in Sec. V.

II. EXPERIMENTAL METHOD

The experiment begins by creating a D_2 plasma in a duoplasmatron ion source. A beam of negative particles is extracted from the source by floating the duoplasmatron to a potential of $U_s \approx -10$ kV. Using charge-to-mass analysis, we form a D^- beam which we further shape and direct into a floating cell at a negative potential U_f. Upon entering the cell, the anions slow down. They are then crossed with a 975-nm laser beam which photodetaches ~10% of the D^-. This creates a beam of ground state, neutral atomic D with a kinetic energy of $\approx -e(U_s - U_f)$, where e is the unit charge. The resulting self-merged, anion-neutral beams exit the floating cell, whereupon the anions return to their initial kinetic energy of $\approx -eU_s$, while that of the neutral atoms remains fixed at $\approx -e(U_s - U_f)$. The exact details are given in Ref. [2]. We varied U_f to set the relative energy E_r.

The merged beams continue into the interaction region where D_2 is formed with a kinetic energy of ≈20 keV. The beginning of this region is defined by a chopping electrode which can be used to deflect the anions and prevent them from

entering the interaction region. We chop the neutrals on and off by switching the laser on and off. By chopping both beams out of phase, we are able to extract any signal D_2 generated in the interaction region from background generated anywhere in the apparatus. Beam profile monitors near the beginning and end of the interaction region allow us to measure the profile of each beam and determine the average overlap form factor of the two beams $\langle\Omega(z)\rangle$ along the z axis set by the trajectory of the overlapping beams. The end of the interaction region is defined by quadrupole electrodes which deflect the anions into a Faraday cup where the current I_{D^-} is measured. The neutral D and daughter D_2 continue into a helium gas cell where a fraction of each are ionized by electron stripping forming $\approx$10 keV D^+ and $\approx$20 keV D_2^+. The remaining neutrals and resulting cations pass into an electrostatic analyzer which consists of a series of cylindrical deflectors. A hole in the outer plate of the lower cylindrical deflector allows the neutral D (and the $\sim 10^{-9}$ smaller amount of D_2) to pass through and continue into a neutral particle detector where we measure the D particle current I_D, expressed in amperes. The voltages on the lower and upper cylindrical deflectors are set to direct the $\approx$20 keV D_2^+ ions onto a channel electron multiplier (CEM) where their rate is measured and recorded as a function of the chopping pattern.

The experiment measures the AD cross section σ_{AD} times the relative velocity between the two beams v_r convolved with the energy spread of the experiment. The energy spread is described in detail in Ref. [2]. The resulting rate coefficient is given by

$$\langle\sigma_{AD} v_r\rangle = \frac{1}{\sigma_{st} N_{He}} \frac{S}{T_a T_g \eta} \frac{e^2}{I_{D^-} I_D} \frac{v_{D^-} v_D}{L\langle\Omega(z)\rangle}. \tag{11}$$

Here σ_{st} is the stripping cross section for D_2 on He; N_{He} is the helium column density in the gas cell; S is the background-subtracted D_2^+ signal corrected for collisionally induced signal loss in the gas cell and energy analyzer; T_a is the transmittance of the energy analyzer; T_g is the transmittance of the grid in front of the CEM; v_{D^-} and v_D are the velocities of the D^- and D beams, respectively; and L is the length of the interaction region. Using our experimental energy spread and the theoretical results described below, we find that the cross section can be accurately extracted from the measured rate coefficient as

$$\sigma_{AD} = \frac{\langle\sigma_{AD} v_r\rangle}{\langle v_r\rangle}, \tag{12}$$

with $\langle v_r\rangle$ averaged over the experimental velocity distribution in the center of mass frame.

Table I lists the experimental nonstatistical uncertainties. Throughout this paper, all uncertainties are given at an estimated 1σ statistical confidence level. We give the errors for our present D results as well as our previous H results for comparison. All uncertainties are treated as uncorrelated and added in quadrature.

When comparing results within a given isotope, the relative error is given by the uncertainties in the background subtraction, beam current measurements, and overlap of the beams. This sum is 12% for each isotope and is dominated by the neutral detector calibration which uses the method outlined in Ref. [3] for H. The detector efficiency for D was calibrated by passing a D^- beam through the helium gas cell as a function of helium pressure and recording both the transmitted D^- and the neutral detector signal. A small correction needs to be made for the unmeasured D^+ generated in the gas cell. For this we used the velocity matched H^- cross sections from Refs. [17,18] for the required D^- single and double electron detachment cross sections. The uncertainties in the detachment cross sections have an insignificant effect on the measured calibration. The dominant uncertainty in the neutral detector calibration is due to the reproducibility of the measured efficiencies.

TABLE I. Summary of nonstatistical experimental uncertainties at an estimated 1σ confidence level. Uncertainties are treated as uncorrelated and added in quadrature. The errors for reaction (1) and (2) are listed separately.

Source	H(%)	D(%)
Background subtraction	5	5
Anion current	3	3
Neutral current	10	10
Overlap of beams	3	3
Relative error within an isotope	12	12
Stripping cross section	16	17
Effects of unknown rovibrational population	10	10
Signal attenuation	1	2
Relative error between isotopes	22	22
Analyzer transmittance	1	1
Grid transmittance	1	1
CEM detection efficiency	2	2
Overlap length	1	1
Helium gas cell column density	7	7
Total nonstatistical uncertainty	24	24

In order to make comparisons between isotopes, one needs to take into account uncertainties that vary between the data sets. These include σ_{st}, the effects of the unknown rovibrational population of the molecules formed, and the collisional destruction of the signal cations before detection. For σ_{st} of D_2 we used the velocity matched results of Ref. [19] for H_2 yielding $(7.7 \pm 1.3) \times 10^{-17}$ cm^2. We corrected for the collisional destruction of the signal D_2^+ using the approach described in Ref. [3]. For the necessary destruction cross section we used the velocity matched results for H_2^+ on He from Ref. [20]. The quadrature sum for the relative error is 22%.

The total nonstatistical error of our measurements for both isotopes is 24% at an estimated 1σ statistical level. This reflects the quadrature sum of all uncertainties listed in Table I. The measurement uncertainties are reviewed in further detail in Refs. [1–3].

III. THEORETICAL METHOD

A. Cross section calculations

The AD cross section calculations for reaction (2) are essentially the same as our previous work for reaction (1) [3]. The basic framework is the nonlocal resonance model described in Ref. [4]. The incoming $H^- + H$ particles move in the attractive potential of the H_2^- $^2\Sigma_u^+$ state, until they penetrate into the $H_2 + e^-$ electronic continuum by crossing

TABLE II. AD cross sections σ_{AD} as a function of relative collision energy $\langle E_r \rangle$. The quoted error represents the 1σ statistical uncertainty.

	σ_{AD} (10^{-16} cm^2)					
	H			D		
$\langle E_r \rangle$ (eV)	Experiment	Error	Theory	Experiment	Error	Theory
0.00374	456	25.4	340	494	39.5	340
0.00418	476	36.1	331	421	60.2	330
0.00524	370	22.1	313	451	33.6	311
0.00665	348	27.3	294	371	48.2	293
0.00898	303	17.0	270	365	26.3	270
0.0119	251	19.9	240	321	38.3	244
0.0155	222	12.3	203	285	19.3	212
0.0197	212	15.9	171	250	29.1	170
0.0245	177	9.64	140	218	15.2	138
0.0300	142	11.8	116	162	19.8	115
0.0361	129	6.52	97.6	147	11.0	96.2
0.0428	96.9	8.96	83.3	111	16.7	81.9
0.0501	84.3	6.13	71.9	105	7.65	70.5
0.0580	68.2	6.81	62.7	83.1	13.0	61.3
0.0666	59.6	5.24	55.1	65.4	7.36	53.8
0.0758	57.7	6.14	48.9	74.0	11.2	47.6
0.0856	47.7	2.92	43.6	65.5	5.27	42.4
0.0961	49.5	5.63	39.2	–	–	–
0.107	42.3	3.59	35.4	47.1	7.08	35.0
0.131	31.9	2.22	29.3	48.0	4.53	29.2
0.158	39.3	3.67	24.7	–	–	–
0.187	23.2	1.87	21.1	38.0	5.13	21.5
0.218	24.5	2.46	19.0	–	–	–
0.252	18.9	1.56	17.1	24.1	3.94	16.9
0.289	19.0	1.54	15.4	–	–	–
0.328	15.0	1.46	14.0	19.4	3.44	14.0
0.369	18.6	1.66	12.8	–	–	–
0.413	13.9	1.30	11.7	17.8	3.26	11.8
0.460	14.7	1.50	10.8	–	–	–
0.509	10.5	1.17	10.0	15.5	2.98	10.1
0.560	10.1	1.40	9.39	–	–	–
0.614	9.46	1.13	8.88	16.0	2.49	9.07
0.671	9.09	1.20	8.50	–	–	–
0.730	9.18	1.01	8.22	11.4	2.08	8.86
0.791	9.83	0.892	8.06	–	–	–
0.855	7.71	0.890	7.96	14.1	1.96	8.50
0.922	6.57	1.09	7.71	–	–	–
0.991	6.30	0.821	7.38	12.3	1.86	7.55
1.06	7.56	0.953	6.98	–	–	–
1.14	8.08	1.84	6.53	5.85	2.10	6.57
1.21	6.01	0.875	6.04	–	–	–
1.29	6.36	1.50	5.51	–	–	–
1.37	4.48	0.738	4.97	–	–	–
1.46	4.95	1.14	4.42	5.29	1.67	4.27
1.54	5.07	0.565	3.88	–	–	–
1.63	3.29	0.908	3.35	–	–	–
1.72	3.16	0.666	2.85	–	–	–
1.82	1.98	0.761	2.38	1.85	1.13	1.97
1.91	1.02	0.689	1.96	–	–	–
2.01	0.774	0.861	1.58	–	–	–
2.12	1.62	0.579	1.26	–	–	–
2.22	1.74	0.822	0.994	−0.09	1.09	0.540
2.33	0.572	0.527	0.781	–	–	–
2.44	1.28	0.469	0.619	–	–	–
2.55	1.08	0.318	0.502	–	–	–

TABLE II. *Continued.*

	σ_{AD} (10^{-16} cm^2)					
	H			D		
$\langle E_r \rangle$ (eV)	Experiment	Error	Theory	Experiment	Error	Theory
2.66	0.564	0.463	0.420	2.51	1.51	0.176
2.78	0.880	0.316	0.358	–	–	–
2.90	1.27	0.401	0.299	–	–	–
3.02	0.628	0.282	0.219	–	–	–
3.14	0.585	0.565	0.218	2.87	1.45	0.0780
3.27	0.222	0.311	0.198	–	–	–
3.40	0.782	0.331	0.183	–	–	–
3.53	0.722	0.397	0.173	–	–	–
3.66	0.698	0.465	0.167	–	–	–
3.80	−0.068	0.364	0.163	–	–	–
3.94	0.390	0.377	0.161	–	–	–
4.22	0.136	0.322	0.161	–	–	–
4.52	0.328	0.303	0.163	–	–	–
4.83	0.141	0.261	0.168	–	–	–

the potential energy curve of the H_2 $^1\Sigma_g^+$ state. The dynamics of nuclear motion are described by the nonlocal energy dependent potential [4,21]. In Ref. [3] we extended this picture to include the contributions of the repulsive H_2^- $^2\Sigma_g^+$ state, in a similar way as Belyaev *et al.* [22], which increases the cross section by about 15% for energies $\gtrsim$0.75 eV.

There are really only two significant differences in the theoretical description for the $D^- + D$ collisions versus the $H^- + H$ case. First, the reduced mass is about two times larger for the deuterated case. This number is easily included in the new calculation, leading to a larger number of partial wave contributions and a larger number of rovibrationally excited D_2 states produced compared to H_2. Second, the deuteron is a boson with spin 1 as compared to spin 1/2 in the case of the fermionic proton. This leads to a different nuclear spin weighting factor for deuterium as compared to hydrogen.

Lastly, AD can produce molecules in highly rotationally excited states which lie above the separate atom limit but are metastable due to the angular momentum centrifugal barrier [3]. These orbiting resonances have angular momentum up to $\approx$30(40) for $H_2(D_2)$ and lifetimes well exceeding the $\approx$1 μs flight time from the interaction region to the detector. Here we included the contribution of these metastable states in our AD cross section calculations, as they contribute to the measured cross section.

B. Scattering simulations of the signal ions

We have investigated the possible scattering effects on the signal H_2^+ and D_2^+ generated by stripping of the AD products in the He gas cell. The scattering cones for each ion could differ, resulting in unequal collection efficiencies for the H_2^+ and D_2^+ signal. Measured from the midpoint of the gas cell, the half angle for the geometric acceptance angle of our CEM is 0.4°, though the actual acceptance half angle is likely to be larger due to focusing effects in the electrostatic analyzer.

Scattering calculations were performed from an electron nuclear dynamics approach. This method uses a time dependent variational principle to derive an approximation to the time-dependent Schrödinger equation (see Refs. [23,24] for further details). The simulations indicate that 97% of the scattered H_2^+ and 99% of the scattered D_2^+ are contained within the CEM half-angle cone of 0.4°. Here we make the assumption that these numbers are 100%, an approximation which has an insignificant effect on the total experimental uncertainty.

IV. RESULTS AND DISCUSSION

The measured H and D data were first collected in November of 2008 using the approach of Refs. [1,2]. Then, using the approach of Ref. [3], the H data were remeasured from January to July of 2010 and the D data from March to July of 2011. Good agreement between the two approaches was found for the H data [3] and we merged the sets together using a statistically weighted averaging method. The D data sets show similar good agreement and we have merged the two data sets using the same averaging method as for the H data. This level of agreement between data sets collected using slightly different approaches and spanning nearly three years gives us a high degree of confidence in the stability of the apparatus over this time.

Our results for reactions (1) and (2) are shown in Fig. 1. The results in red are for deuterium and those in black for hydrogen. The error bars display the 1σ statistical error of the experimental results. The data for hydrogen and deuterium are also presented in Table II. Additionally, we plot the Langevin value [4,25]. This has been reduced by a factor of 2 to take into account that AD proceeds primarily via the H_2^- $^2\Sigma_u^+$ state and the contribution of the $^2\Sigma_g^+$ state is negligible to first order.

Table II presents the cross sections for these reactions in units of cm^2. In Fig. 1, though, we have multiplied the cross section data by $\langle E_r \rangle^{1/2}$. This effectively removes any Langevin-like behavior in the cross section [25]. Were the reaction truly Langevin-like, the resulting $\sigma_{AD}\langle E_r \rangle^{1/2}$ would be independent of $\langle E_r \rangle$. The structure shown in Fig. 1 demonstrates the remaining non-Langevin behavior in the reaction. For energies between $\sim$3 meV and $\sim$1 eV the reaction is faster than Langevin. This is caused by the fact that the

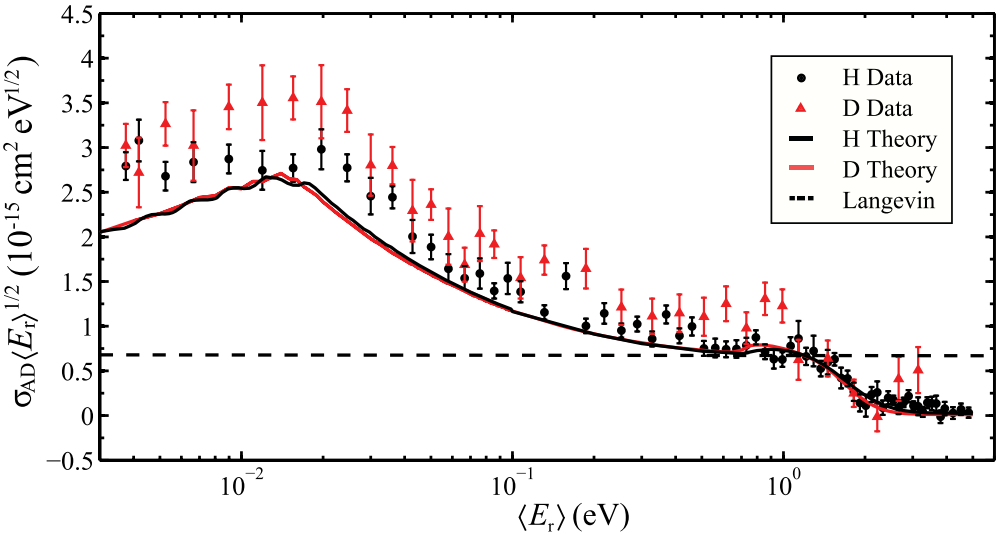

FIG. 1. (Color) Scaled AD cross section versus relative collision energy for reaction (1) is shown in black and for reaction (2) in red. The filled circles are the measured results for the hydrogen and the filled triangles for deuterium. The error bars on each point give the associated 1σ statistical error. The solid curves present our theoretical results, while the dashed line is the Langevin value.

long range interaction potential for $H^- + H$ at distances of $3a_0 - 20a_0$ is much more attractive than indicated by the dipole polarizability of the hydrogen atom. Above ~1 eV, the reaction rapidly turns off due to the opening of the collisional detachment channel

$$H(D)^- + H(D) \rightarrow H(D) + H(D) + e^-, \qquad (13)$$

a process which is not accounted for by the Langevin cross section.

As discussed earlier, theory predicts no significant isotope effect in the total cross section for reactions (1) and (2). Comparing only the two experimental data sets, our measured results are also consistent with there being no isotope effect in the total AD cross section. For a quantitative comparison we focus on energies $\lesssim$0.75 eV, where AD can proceed only via the attractive $^2\Sigma_u^+$ state and which is also below the threshold for collisional detachment [Eq. (13)]. The ratio of the D to H data sets is 1.21 ± 0.03, which is effectively within the estimated 22% relative error between the isotopes.

Comparing the theoretical to the experimental results, for the corresponding energies below 0.75 eV, yields ratios of 0.84 ± 0.01 for the H data and 0.70 ± 0.06 for the D data. With an estimated total nonstatistical uncertainty of 24%, we find good agreement between theory and experiment for the H data, as has been previously reported [1–3]. For the D data, the experimental results differ from theory only at an $\approx 1.25\sigma$ level, which we interpret as being in agreement.

As discussed in the Introduction the lack of an isotope effect is related to both the fast autodetachment rate at small internuclear separations of H^- and H and the fact that the trajectories depend only on the energy and not the mass of the particles. That said, the calculations do indicate that there is a small isotope effect due to nuclear spin at low energies. Additionally, at energies $\gtrsim$0.75 eV, the small differences seen in the predicted cross sections are due to threshold effects associated with opening of the $H(D) + H(D) + e^-$ channel and due to the contribution of the repulsive $^2\Sigma_g^+$ state. These differences are too small to be discernible in our measurements.

V. CONCLUSION

Previous experimental and theoretical work has demonstrated the existence of a large isotope effect for the partial AD cross section of diatomic collision systems. Our theoretical results show no such effect in the total AD cross section for the $H^- + H$ and $D^- + D$ systems studied here. The new experimental data are consistent with this as well as with both the energy dependence and magnitude of the theoretical calculations. Taken all together, our results indicate that though the predicted rovibrational distribution of flux is different for each system, the total flux is essentially the same. We expect to see similar behavior for the AD isotope effect in other collision systems possessing an attractive long range potential where autodetachment is essentially forbidden leading to a region where fast autodetachment turns on and stays on.

ACKNOWLEDGMENTS

The authors thank M. Hahn for stimulating discussions. This work was supported in part by NSF Grants No. CHE-0520660, No. AST-0606960, and No. AST-0807436. H.B. was supported in part by the German academic exchange service DAAD. M.Č. and J.E. were supported in part by Grant No. GACR 208/10/1281 from the Czech Republic. X.U. acknowledges support from the Fund for Scientific Research (FNRS).

[1] H. Kreckel, H. Bruhns, M. Čížek, S. C. O. Glover, K. A. Miller, X. Urbain, and D. W. Savin, Science **329**, 69 (2010).

[2] H. Bruhns, H. Kreckel, K. A. Miller, X. Urbain, and D. W. Savin, Phys. Rev. A **82**, 042708 (2010).

[3] K. A. Miller, H. Bruhns, J. Eliášek, M. Čížek, H. Kreckel, X. Urbain, and D. W. Savin, Phys. Rev. A **84**, 052709 (2011).
[4] M. Čížek, J. Horáček, and W. Domcke, J. Phys. B **31**, 2571 (1998).
[5] S. Živanov, M. Čížek, J. Horáček, and M. Allan, J. Phys. B **36**, 3513 (2003).
[6] M. A. Smith and S. R. Leone, J. Chem. Phys. **78**, 1325 (1983).
[7] M. Čížek, J. Horáček, F. A. U. Thiel, and H. Hotop, J. Phys. B **34**, 983 (2001).
[8] D. Rapp, T. E. Sharp, and D. D. Briglia, Phys. Rev. Lett. **14**, 533 (1965).
[9] G. J. Schulz and R. K. Asundi, Phys. Rev. Lett. **15**, 946 (1965).
[10] E. Krishnakumar, S. Denifl, I. Čadež, S. Markelj, and N. J. Mason, Phys. Rev. Lett. **106**, 243201 (2011).
[11] M. Allan and S. F. Wong, Phys. Rev. Lett. **41**, 1791 (1978).
[12] J. Horáček, M. Čížek, K. Houfek, P. Kolorenč, and W. Domcke, Phys. Rev. A **70**, 052712 (2004).
[13] Y. Xu and I. I. Fabrikant, Appl. Phys. Lett. **78**, 2598 (2001).
[14] K. Houfek, M. Čížek, and J. Horáček, Phys. Rev. A **66**, 062702 (2002).
[15] J. P. Gauyacq, *Dynamics of Negative Ions*, Lecture Notes in Physics Vol. 15 (World Scientific, Singapore, 1987).
[16] H. Bruhns, H. Kreckel, K. Miller, M. Lestinsky, B. Seredyuk, W. Mitthumsiri, B. L. Schmitt, M. Schnell, X. Urbain, M. L. Rappaport, C. C. Havener, and D. W. Savin, Rev. Sci. Instrum. **81**, 013112 (2010).
[17] T. J. Kvale, J. S. Allen, X. D. Fang, A. Sen, and R. Matulioniene, Phys. Rev. A **51**, 1351 (1995).
[18] Atomic Data for Fusion. Vol. 1, edited by C. F. Barnett, Oak Ridge National Laboratory Report No. ORNL-6086, 1, F-12 (1990), http://www-cfadc.phy.ornl.gov/redbooks/redbooks.html.
[19] R. Browning, C. J. Latimer, and H. B. Gilbody, J. Phys. B **3**, 667 (1970).
[20] Y. Suzuki, T. Kaneko, M. Tomita, and M. Sakisaka, Phys. Soc. Jpn. **55**, 3037 (1986).
[21] W. Domcke, Phys. Rep. **208**, 97 (1991).
[22] A. K. Beylaev, A. S. Tiukanov, and W. Domcke, Chem. Phys. **325**, 378 (2006).
[23] R. Cabrera-Trujillo, Y. Öhrn, E. Deumens, and J. R. Sabin, J. Chem. Phys. **116**, 2783 (2002).
[24] E. Deumens, A. Diz, H. Taylor, and Y. Öhrn, J. Chem. Phys. **96**, 6820 (1992).
[25] G. Gioumousis and D. P. Stevenson, J. Chem. Phys. **29**, 294 (1958).